Materials Advances

ROYAL SOCIETY OF CHEMISTRY

PAPER

View Article Online
View Journal | View Issue

Check for updates

Cite this: *Mater. Adv.*, 2025, 6, 7919

Exploring the dual role of TEMPO-oxidized cellulose nanofibers in CdSe quantum dot synthesis for biocomposites in metal ion chemosensing

Mauricio C. Cifuentes,[ab] Daniel A. Amaya,[a] Cristian Blanco-Tirado[a] and Marianny Y. Combariza*[a]

Received 1st July 2025,
Accepted 6th September 2025

DOI: 10.1039/d5ma00700c

rsc.li/materials-advances

TEMPO-oxidized cellulose nanofibers (TOCNs) are commonly used to develop hybrid functional materials. Aldehyde moieties in TOCNs allow them to act as reducing agents for the *in situ* synthesis of Ag, Pt, Au, and Pd NPs (NPs). However, no reports exist on using TOCNs as reducing agents for synthesizing semiconducting quantum dots (QDs). This study presents the simultaneous use of TOCNs as a reducing and stabilizing agent for synthesizing thioglycerol CdSe QD (QTC) biocomposites. In the presence of TOCNs, the synthesis of CdSe–TG QDs proceeds rapidly, eliminating the need for an additional reducing agent. TEM analysis shows that a thirty-minute reaction at 100 °C in aqueous media containing TOCNs produces homogeneously dispersed CdSe–TG QD biocomposites with a crystallite size of approximately 2.3 nm, whereas a reaction without TOCNs using $NaBH_4$ as a reducing agent takes 12 to 15 hours and results in larger nanostructures. QTC bionanocomposites were tested as chemosensors for metal ion detection in water using absorption and fluorescence spectroscopy. The hybrid material displayed high selectivity and sensitivity toward copper ions (Cu^{2+}) with a detection limit as low as 320 ppb.

Open Access Article. Published on 11 September 2025. Downloaded on 12.05.2026 23:40:00.
This article is licensed under a Creative Commons Attribution-NonCommercial 3.0 Unported Licence.

Introduction

Quantum dots (QDs) are light-emitting inorganic semiconductor materials with attractive electronic and optical properties. High quantum yields, strong resistance to photodegradation, broad extinction spectra, narrow and tunable fluorescence emission, among other characteristics, make them promising materials for photocatalysis, solar cells and, sensing applications.[1–3] QDs prepared *via* an organometallic synthetic route are typically stabilized by hydrophobic capping agents such as trioctylphosphine oxide (TOPO), trioctylphosphine (TOP), or hexadecylamine (HDA). These agents help provide highly crystalline and monodisperse nanomaterials. However, they also impact the water dispersibility of QDs, and have been associated with toxicity, limiting their practical use in aqueous media.[4–6] These challenges can be addressed by substituting the hydrophobic ligand with hydrophilic molecules, although there are some concerns about potential alterations in photoluminescence.[7,8]

Greener approaches to chalcogenide QDs involve reacting metallic precursors (*e.g.*, zinc, cadmium, and silver) with the corresponding chalcogen precursor (*e.g.*, tellurium, sulfur, and selenium) in the presence of diverse capping agents (3-mercaptopropionic acid, 1-thioglycerol, glutathione, and L-cysteine).[9–14] These approaches require dissolving the metal precursor and the capping agent in degassed water, followed by rapidly injecting the chalcogenide precursor at high pH (9–11). Subsequently, the system is refluxed, and crystal growth is controlled by reaction time.[9] Cadmium selenide (CdSe) QDs are classic II–VI semiconducting nanomaterials with a band gap of 1.74 eV at room temperature.[15,16] Due to their high crystallinity and photoluminescence properties, these QDs are widely used in applications like solar cells, chemosensors, and biomedical imaging[16–18] However, the synthesis of CdSe QDs requires reducing agents, like $NaBH_4$, and long reaction times.[3,19,20]

Cellulose, the most abundant natural polymer on earth, has unique characteristics such as high biocompatibility, hydrophilicity, relative thermal stability, mechanical strength, high sorption capacity, and self-assembly properties. Traditionally used in textiles and papermaking, cellulose now has applications in more technical areas, such as wastewater treatment, enhanced oil recovery, and high-performance advanced biomaterials, among others.[21] The presence of hydroxyl groups on the cellulose surface gives the polymer remarkable chemical flexibility and the ability to introduce a wide range of functionalities to control interfacial phenomena.[22,23]

[a] *Escuela de Química, Universidad Industrial de Santander, Bucaramanga, 680002, Colombia. E-mail: marianny@uis.edu.co*
[b] *Facultad de Ciencias Naturales e Ingeniería, Unidades Tecnológicas de Santander, Bucaramanga, 680005318, Colombia*

© 2025 The Author(s). Published by the Royal Society of Chemistry

Open Access Article. Published on 11 September 2025. Downloaded on 12.05.2026 23:40:00.
This article is licensed under a Creative Commons Attribution-NonCommercial 3.0 Unported Licence.

Nanocelluloses, as nanofibers and nanocrystals, are a new class of cellulosic derivatives with remarkable physicochemical properties and applications. Chemical, mechanical, and biological processes, as well as their combinations, have been extensively studied for the isolation of nanocellulose, as documented in numerous literature reviews.[24–26] One of the most widely used chemical methods for producing cellulose nanofibers is TEMPO-mediated oxidation. In this catalytic regioselective reaction, the primary –OH groups at the C6 position of the anhydroglucose units in cellulose are sequentially oxidized to aldehydes and then to carboxylic acids.[27] The reaction results in what is known as TEMPO-oxidized cellulose nanofibers (TOCNs).

The role of TOCNs as a stabilizing agent for CdS QDs was recently reported. $CdCl_2$ and Na_2S precursors were mixed with TOCNs to form films of TOCN-containing CdS QDs formed *in situ*. These composites exhibited a transmittance of up to 95% at 550 nm and an elastic modulus of up to 8.1 GPa, indicating their potential for use in flexible electronic devices. In this context, there is no change in the oxidation state from precursors to products in the synthesis of CdS QDs; thus, TOCNs act as a stabilizing agent. This is not surprising, as cellulose derivatives are known for their ability to prevent nanoparticle aggregation and decomposition.[28] Additionally, CdTe QDs were immobilized and stabilized using bacterial cellulose and incorporated into cellulose microspheres by mechanically spraying a mixture of QDs and TOCNs. In these examples, $NaBH_4$ was always used as a reducing agent to reduce the precursor from Te^{4+} to Te^{2-}.[29–31]

Recent reports, including our research, demonstrate that TOCNs can reduce and stabilize metallic NPs.[32,33] For example, in TOCN-based hydrogels prepared by adding $AgNO_3$ aqueous solutions to TOCN suspensions, Ag^+ ions were observed to be reduced to metallic silver by interacting with the unreacted aldehydes on the TOCN surfaces and the reducing end of the cellulose.[34] In this example, TOCNs effectively reduced silver ions, which have a standard reduction potential of +0.7996 V ($Ag^+|Ag^0$). Considering that the reduction potential of $Se^{4+}|Se^{2-}$ is +0.190 V, we hypothesized the possibility of obtaining *in situ* CdSe QDs by reducing selenium ions in the precursor Na_2SeO_3 from Se^{4+} to Se^{2-} using only TOCNs, without the need for any additional reducing agents.[35]

We report the successful synthesis of a luminescent CdSe–TG QDs/TOCN bionanocomposite in aqueous media using a one-pot strategy. In this process, cellulose nanofibers eliminate the need for a reducing agent, which is typically required for producing these materials. When TOCNs were exclusively used as a reducing and stabilizing agent, homogeneous and well-dispersed CdSe QDs were obtained. Furthermore, the reaction time decreased from 12 hours, required for synthesizing water-dispersed CdSe TG QDs using $NaBH_4$, to just 0.5 hours with TOCNs.[3,36] To test the role of TOCNs as a reducing agent, post-oxidation of TOCNs was performed to convert the remaining aldehydes into carboxylic acid groups and thereby assess the reducing capability of aldehydes in producing *in situ* CdSe QDs. No formation of semiconducting CdSe QDs was observed when using post-oxidized TOCNs, despite prolonging the reaction for 6 hours.

Materials and methods

Chemicals

Fique fibers (Furcraea macrophylla) were collected in San Joaquin, Santander, Colombia. 2,2,6,6-Tetramethyl-piperidin-1-oxyl (TEMPO) was obtained from Sigma Aldrich. Sodium hypochlorite (NaClO, 13%) was sourced from Carlo Erba Reagents (Milan, Italy). Sodium bromide (NaBr), hydrogen peroxide (H_2O_2), sodium hydroxide (NaOH), ethanol (EtOH), hydrochloric acid (HCl, 37%), thioglycerol ($C_3H_8O_2S$), sodium selenite (Na_2SeO_3), and cadmium acetate dihydrate ($Cd(CH_3COO)_2{\cdot}2H_2O$) were acquired from Merck (Darmstadt, Germany). All chemical reagents were used as received, with no additional purification. Aqueous solutions and suspensions were prepared with ultrapure water (18 MΩ cm/25 °C).

Fique tow treatment, delignification, and TOCN extraction

TOCN isolation was performed according to procedures previously reported by our group, with slight modifications.[34] Fique fibers were immersed for 30 minutes at 25 °C in an ultrasonic bath (Bransonic CPX3800, 40 kHz, 130 watts) containing deionized water and then dried to eliminate impurities. Twenty-four grams of short fique fibers were immersed in 300 mL of a H_2O_2 solution (10% w/w) at pH 11.5 to remove hemicellulose and lignin. To optimize the process, this step was repeated twice. The mixture was maintained in an ultrasonic bath for 2.5 hours at 70 °C and then dried in an oven.

For TOCN extraction, delignified fique tow was suspended in 200 mL of water. TEMPO (32 mg) and sodium bromide (200 mg) were gradually added to the suspension. NaClO solution (0.1212 mol) was added dropwise to initiate the oxidation reaction. The reaction was conducted at room temperature in an ultrasonic bath (Bransonic CPX3800, 40 kHz, 130 watts), with the pH maintained at 10.5. The addition of ethanol halted the reaction. The product was centrifuged with ultrapure water until a neutral pH was achieved to remove unreacted species and separate TOCNs. A TOCN aqueous suspension of 1.34 wt% was obtained following mechanical disintegration in an Ultrasonic Processor (Sonics Vibra-cell VC750, 20 kHz, 750 W) for 10 minutes (1 : 1 pulses) at an amplitude of 40%.

Synthesis of thioglycerol-functionalized CdSe–TG quantum dots (QTG)

The synthesis of CdSe–TG quantum dots was performed using a previously reported method with some modifications.[3] A solution of cadmium acetate dihydrate (1.54 g) and thioglycerol (TG, 1 mL) in 200 mL of degassed water was continuously stirred under an argon atmosphere. The pH of the resulting mixture was adjusted to 11.2 with a 2 M NaOH solution. Separately, an aqueous solution of Na_2SeO_3 was prepared by dissolving 0.5 g in 5 mL of water and injected into the pH-controlled mixture of Cd^{2+} and TG while stirring vigorously.

© 2025 The Author(s). Published by the Royal Society of Chemistry

Open Access Article. Published on 11 September 2025. Downloaded on 12.05.2026 23:40:00.
This article is licensed under a Creative Commons Attribution-NonCommercial 3.0 Unported Licence.

The molar ratio of Cd^{2+}/TG/Se^{2-} was set at 1 : 2 : 0.5. Next, a solution of the reducing agent $NaBH_4$ (0.5 g in 5 mL) was injected into the final solution using a syringe, while it was continuously stirred at 100 °C under an argon atmosphere. The reaction proceeded for 12, 18, and 24 h, until it turned yellow. The QDs were extracted by precipitation in isopropanol. The solution was stirred for one hour, and the precipitate was centrifuged and then dried in a desiccator under vacuum. The materials prepared with 12-, 18-, and 24-hour reaction times are labelled as QTG-1, QTG-2, and QTG-3, respectively.

In situ synthesis of the CdSe–TG QDs/TOCN (QTC) biocomposite

The synthesis of CdSe–TG quantum dots/TOCNs followed the procedure described in the previous paragraph, with the distinction that instead of using $NaBH_4$ as the reducing agent, we added a TOCN solution (20 mL, 1 wt%) as both a stabilizer and reducing agent. The transition from a translucent to a yellow-coloured solution indicates the formation of a CdSe–TG QDs/TOCN bionanocomposite. The TOCNs' aldehyde content was determined through conductometric analyses, and the molar ratios of Cd2+/TG/Se^{2-}/COH were established as 1 : 2 : 0.5 : 1.5. Reaction times of 30, 60, and 90 minutes were selected based on previous tests. CdSe–TG QDs/TOCNs were isolated using isopropanol. This product was re-dispersed in deionized water and lyophilized to obtain an aerogel material. The materials prepared with reaction times of 30, 60, and 90 minutes were labelled as QTC-30, QTC-60, and QTC-90, respectively.

Metal ion detection assay

The selectivity and sensitivity of the bionanocomposites' chemosensing properties were tested for M^{x+} metal ions, including Cu^{2+}, Ca^{2+}, Mg^{2+}, Fe^{3+}, Ni^{2+}, Zn^{2+}, and Cd^{2+}. Sensitivity was assessed using aliquots of M^{x+}, ranging from 0 to 18 ppm, added to a 2 mL aqueous solution of the QTC (1000 ppm) bionanocomposite, with both absorbance and fluorescence spectra recorded. Selectivity was evaluated under the same conditions for aqueous solutions containing mixtures of the metals.

Quantum yield determination

The quantum yields were obtained by using anthracene as a reference (φ_F = 0.29 in ethanol at 390 nm) and using the following equation:

$$\varphi_{f,x} = \varphi_{f,st} \times \frac{F_x}{F_{st}} \times \frac{1 - 10^{-A_{st}L_{st}}}{1 - 10^{-A_xL_x}} \times \frac{{\eta_x}^2}{{\eta_{st}}^2} \quad (1)$$

where x represents the sample solution, st represents the standard solution, φ represents the quantum yield, F represents the integrated area of the emission, A represents the absorbance at the excitation wavelength, L represents the length of the cell, and η represents the refractive index of the solvent.[37,38]

Materials characterization

A Shimadzu UV-vis spectrophotometer (UV-2401PC) was used to obtain absorbance measurements ranging from 190 to 1100 nm. A Photon Technology International PTI QuantaMaster fluorescence/luminescence spectrometer covered an emission range of 185 to 680 nm with a focal length of 300 mm for emission measurements. For attenuated total reflectance-infrared (ATR-IR) measurements, a Bruker Tensor 27 (Billerica, MA) FTIR instrument equipped with a Platinum Diamond ATR unit A225/Q (Billerica, MA) was utilized at a resolution of 2 cm^{-1}, accumulating 32 scans for each spectrum. X-ray diffraction (XRD) analyses were conducted using a Bruker D8 DISCOVER X-ray diffractometer (Billerica, MA) with a DaVinci geometry; the instrument featured a CuKa1 radiation source (40 kV and 30 mA), a VANTEC-500 area detector, and a poly(methyl methacrylate) sample holder. Thermogravimetric (TGA) analyses were conducted using an STA 449 F5 Jupiter instrument (São Paulo, Brazil) under a nitrogen flow of 50 mL min^{-1}. The samples were scanned from 30 to 800 °C at a heating rate of 10 °C min^{-1}. The zeta potential was measured with a Malvern Zetasizer Nano ZS90 instrument (Worcestershire, UK), equipped with a capillary cell 1070 and utilized for DLS measurements. Scanning electron microscopy (SEM) analyses were performed using a QUANTA FEG 650 (FEI) instrument equipped with a large field detector. Micrographs were captured at 7 kV; in every case, the sample surfaces were coated with a thin carbon layer before analysis. Elemental analysis was conducted using an energy-dispersive X-ray spectroscopy (EDS) accessory connected to the microscope at 20 kV. Transmission electron microscopy (TEM) analyses were done using an FEI Tecnai G2 F20 instrument at an acceleration of 160 kV.

Results and discussion

Synthesis of QTC bionanocomposites

The synthetic procedure for the *in situ* formation of the CdSe–TG QDs/TOCN bionanocomposite is illustrated in Fig. 1. Lignin and hemicellulose were removed from Fique fibers through a bleaching procedure using an alkaline hydrogen peroxide solution. Cellulose nanofibers (CNFs) were derived from delignified fique tow *via* oxidation. TEMPO-oxidized treatment facilitates regioselective surface oxidation of the primary –OH groups at the C6 position of the glucopyranose rings into aldehydes and, ultimately, carboxylates *via* a catalytic cycle. The TEMPO-oxidized cellulose nanofibers (TOCNs) used in this work contain carboxylate and aldehyde levels of 0.94 and 0.46 mmol g^{-1} cellulose, respectively, and have a ζ potential of −43.4 mV.

When the $Cd(CH_3COO)_2{\cdot}2H_2O$/TG aqueous mixture is added to TOCNs, the carboxylate groups in neighbouring glucopyranose rings can function as cation exchangers, replacing Na^+ ions (leftover from TEMPO oxidation) with Cd^{2+} ions (Fig. 1). Additionally, Cd^{2+} ions can coordinate with adjacent –OH groups at the C2 and C3 positions in the glucopyranose units along the cellulose nanofibril chain.[43] These two interactions facilitate the TG-capped Cd^{2+} ion's anchoring into the layered structure of TOCNs, eventually preventing the aggregation of CdSe QDs and promoting good dispersion of the NPs in the TOCNs. When Na_2SeO_3 is added to the reaction mixture

Open Access Article. Published on 11 September 2025. Downloaded on 12.05.2026 23:40:00.
This article is licensed under a Creative Commons Attribution-NonCommercial 3.0 Unported Licence.

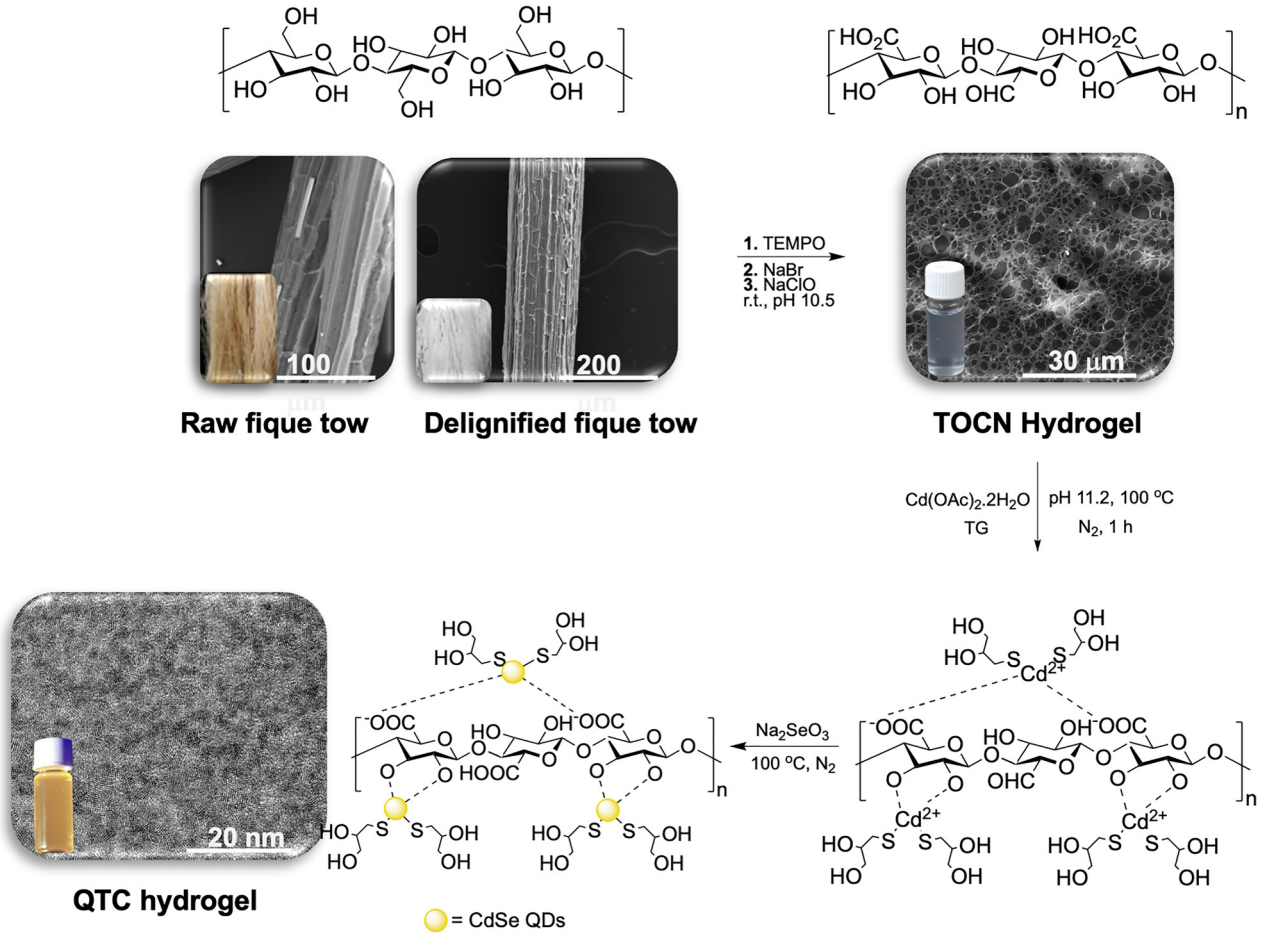

Fig. 1 Synthesis of the CdSe–TG QDs/TOCN bionanocomposite.

containing TOCNs, Se^{4+} is reduced to Se^{2-} to form CdSe QDs. The formation of a yellow colour in the colloidal mixture indicated the formation of CdSe QDs in the reaction mixture containing TOCNs (Fig. 1). During the TEMPO-catalyzed oxidation of cellulose, the primary hydroxyl group at the C6 position of the anhydroglucose unit is initially converted into an aldehyde and subsequently into a carboxylate. However, some aldehydes remain in the cellulosic structure even after the oxidation process stops. These intermediate aldehyde groups (0.46 mmol CHO per g cellulose) function as a reducing agent with an oxidation potential of approximately −0.580 V (R–CHO|R–COOH) to facilitate the reduction of Se^{4+} to Se^{2-} with a reduction potential of +0.19 V.[39–41] Interestingly, while the cadmium precursor (Cd^{2+}) could also be reduced by TOCNs it does not readily undergo reduction because the selenium ion (Se^{4+}) is a stronger oxidizing agent. This is evidenced by the standard reduction potentials: $Se^{4+}|Se^{2-}$ has a potential of +0.19 V, which is more positive than that of $Cd^{2+}|Cd^{0}$ at −0.403 V. Moreover, stabilization of Cd^{2+} ions by chelation with the carboxylate groups of TOCNs could also hinder the reduction of Cd^{2+} to Cd^{0}.[42–44]

Aldehydes have been shown to be effective reducing agents for various metal ions, including platinum, silver, palladium, and gold.[34,45,46] For example, Nath *et al.* found that acetaldehyde (−0.390 V) and formaldehyde (0.056 V) can reduce Au^{3+} to Au^{0} for Au NP synthesis. Acetaldehyde reduced Au^{3+} immediately upon the reaction's initiation, whereas formaldehyde required a longer time due to its lower oxidation potential.[46] Researchers have widely used nanocellulose derivatives to synthesize metal nanoparticles, leveraging the aldehyde and hydroxyl groups in their cellulosic structure. For example, Xu *et al.* used dialdehyde cellulose nanocrystals as both the reducing and stabilizing agents to synthesize silver nanoparticles. Similarly, Battocchio *et al.* harnessed the reducing power of TOCNs to produce the same nanoparticles without the need for additional reducing agents.[47,48]

The production of CdSe–TG QDs with and without TOCNs was monitored using UV-vis and fluorescence spectroscopy. According to Brahim *et al.*, CdSe–TG QDs exhibit two characteristic bands in the region of 370 to 400 nm.[3,49] However, as shown in Fig. 2a, the excitonic absorption band typical of semiconductor nanocrystals appears as a wide band at 370 nm for the QTG QD dispersions, indicating variability in the crystal size distribution. The absorption maxima of these materials remain consistent regardless of the reaction time.[3] On the other hand, the UV-vis spectra of QTC bionanocomposites show two absorption bands

© 2025 The Author(s). Published by the Royal Society of Chemistry

Open Access Article. Published on 11 September 2025. Downloaded on 12.05.2026 23:40:00.
This article is licensed under a Creative Commons Attribution-NonCommercial 3.0 Unported Licence.

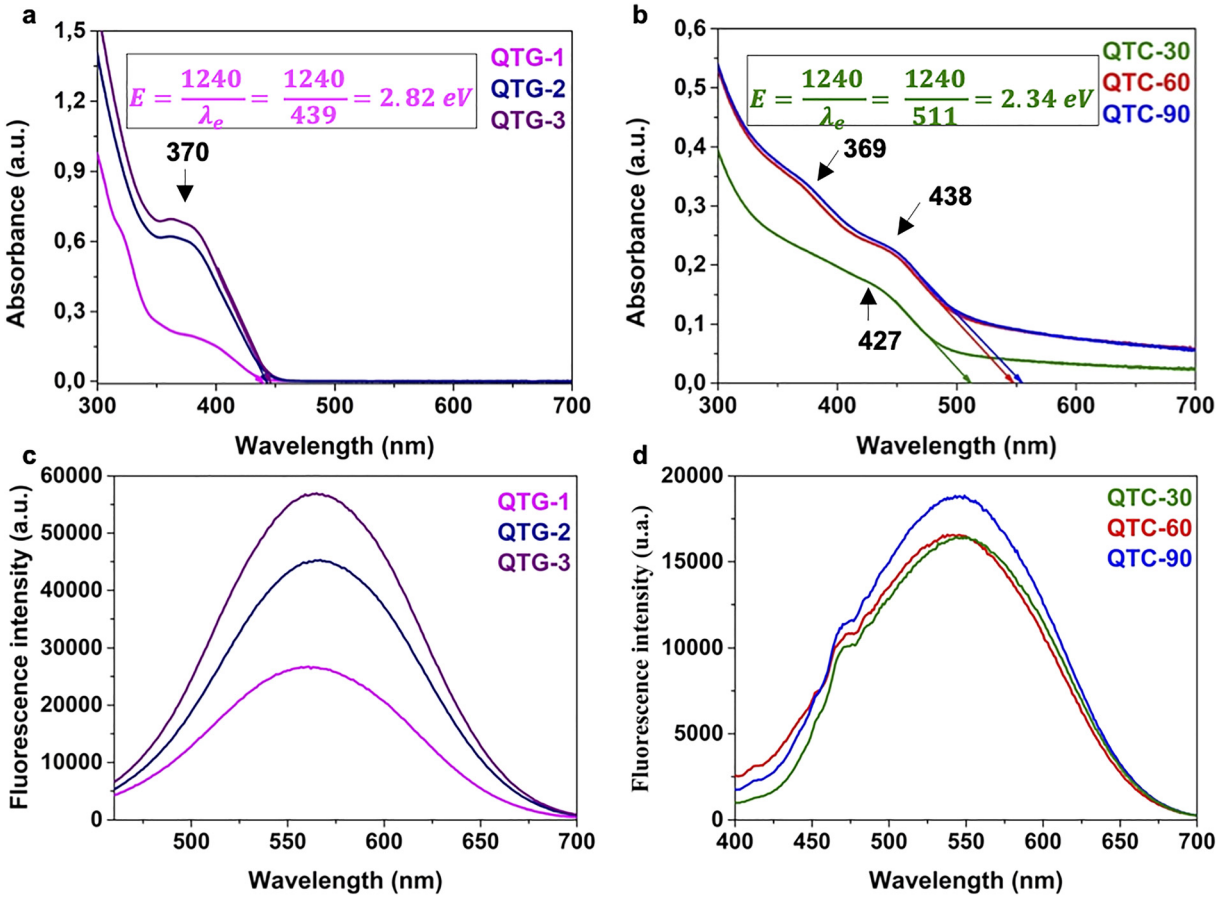

Fig. 2 UV-vis and fluorescence spectra of (a) and (c) QTG bulk QDs and (b) and (d) QTC bionanocomposites, respectively.

between 367 nm and 440 nm. There is a bathochromic shift—from 427 nm to 438 nm—as the reaction time increases from 30 to 60 minutes. This shift results from the quantum confinement effect characteristic of QD formation, which is associated with the increase in crystal size over time as the reaction progresses.[50,51] Extending the reaction time to 90 minutes did not lead to a higher bathochromic shift, which aligns with the crystal size determined from the TEM micrograph (Table S1). In contrast, TOCNs show no absorption (Fig. 2b and Fig. S1, respectively).

Research studies have shown that using modified CNCs can produce CdS QDs that are smaller than those synthesized in bulk.[52,53] Chen *et al.* reported that the carboxyl groups introduced in cellulose nanocrystals (CNCs) by TEMPO oxidation were vital for the controlled synthesis of CdS QDs, as they formed carboxyl-Cd^{2+} complexes prior to the addition of sodium sulfide, enabling the *in situ* formation of the QDs in the CNC matrix. Moreover, partially desulphonated CNCs functionalized with polyethyleneimine led to the formation of smaller-sized CdS QDs, demonstrating the impact of additional capping on the crystal size.[53] TOCNs act as a stabilizing agent, structural template, and ion-exchange matrix during CdSe–TG synthesis. Under alkaline conditions, the carboxylate and hydroxyl groups strongly bind the Cd^{2+} cation, controlling nucleation rates and preventing aggregation during the formation of NPs. In addition, hydroxy and thiol groups from TG contribute to controlling the rate of crystal size formation, stabilizing the growth of QDs, ensuring efficient surface passivation, and improving size uniformity, as observed in the TEM micrographs (Fig. 1 and 4).[28]

The band gap of QTC bionanocomposites and QTG QDs was calculated using the absorption edges (λ_e), which were obtained from the intersection of the sharply decreasing region of the UV-vis spectra with the baseline, as illustrated in Fig. 2a and b.[52] Table S1 in the SI shows a decrease in the band gap from 2.43 eV during the first 30 minutes of reaction time to 2.27 eV and 2.23 eV at 1 hour and 1.5 hours of reaction time, respectively, as the crystal size increases.[54] According to our results, TOCNs exert greater control over QD size distribution, yielding CdSe–TG QDs with an average crystal size of 2.25 nm (QTC-30, E_g = 2.43 eV). In contrast, in the absence of TOCNs, relatively larger nanostructures are produced (QTG-1 with the average size = 2.66 nm, and E_g = 2.82 eV). Additionally, using TOCNs as a reducing agent significantly reduces the synthesis time of CdSe–TG QDs compared to $NaBH_4$, from 18 to 24 hours without TOCNs to about 1.5 hours with nanocellulose (Table 1).[49,55]

To investigate how aldehyde moieties influence the formation of CdSe QDs, TOCNs underwent mild oxidation with $NaClO_2$ to oxidize aldehydes to carboxylates. The resulting material, known as post-oxidized TOCNs, was used to

Open Access Article. Published on 11 September 2025. Downloaded on 12.05.2026 23:40:00.
This article is licensed under a Creative Commons Attribution-NonCommercial 3.0 Unported Licence.

Table 1 Comparative images of QTC bionanocomposites, QTC with post-TOCN, and QTC synthesis without TG at different reaction times

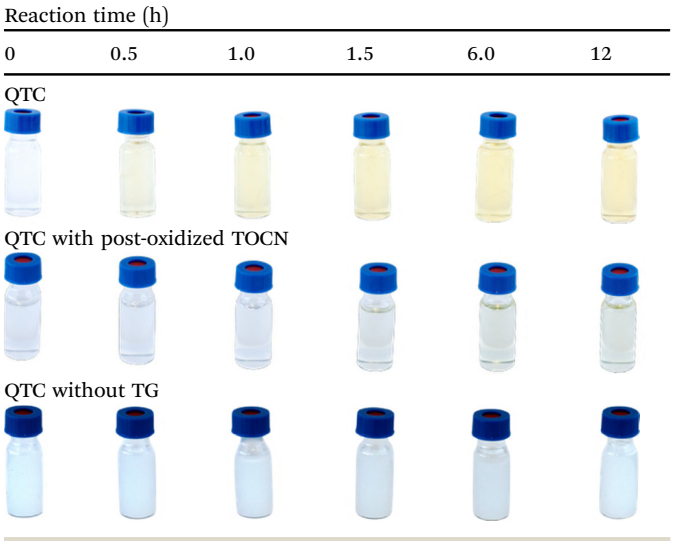

synthesize QTC bionanocomposites under the same reaction conditions as those used for TOCNs. However, no formation of CdSe–TG QDs occurred when using post-oxidized TOCNs, even after 6 hours of reaction time. This finding suggests that the aldehyde groups generated through the incomplete oxidation of cellulose in the catalytic cycle of the TEMPO reaction are crucial for TOCNs to function as an effective reducing agent, thereby reducing the precursor Se^{4+} ions to Se^{2-} in the CdSe–TG QDs.[56] Additionally, the absence of TG as a capping agent resulted in a vivid white solution, illustrated in Table 1, indicative of the interaction between the carboxylate groups of TOCNs and Cd^{2+} ions.

The fluorescence spectra of QTC bionanocomposites and QTG QDs were recorded at an excitation wavelength of 370 nm in an aqueous solution, as illustrated in Fig. 2c and d. The bionanocomposites exhibited maximum emission at 545 nm for the samples with reaction times of 30 and 60 minutes, and at 548 nm for the sample with a 90-minute reaction time. However, the fluorescence emission of the QTC bionanocomposites occurred at a shorter wavelength compared to the CdSe–TG QDs without TOCNs. Like UV-vis observations, the fluorescence emission shifted to longer wavelengths as the reaction time increased, a phenomenon attributed to the quantum confinement effect. Notably, this behavior was observed only for the QTC-90 bionanocomposite. The decrease in fluorescence intensity of QTC bionanocomposites was found to be smaller than that of the QTG QDs solution; this is attributed to the TOCN matrix enhancing the stability of CdSe–TG QDs, as the TOCN surface can prevent agglomerate formation and reduce the number of defects on the QDs surface.

Among the three bionanocomposites obtained, QTC-30 exhibited the highest relative quantum yield in water (φ_F = 0.0206) using anthracene as a reference (φ_F = 0.29). The UV-vis absorption and fluorescence spectra of anthracene solutions (N = 6) and solutions of the prepared bionanocomposites (N = 6) were recorded, and the quantum yield of the latter was calculated according to eqn (1). As the size of the CdSe–TG QDs particles increases, their surface-to-volume ratio decreases, but surface defects increase disproportionately.[57,58] These defects create nonradiative recombination pathways, which reduce the quantum yield. For instance, Kumal *et al.* reported that TOP-capped CdSe QDs exhibited a decrease in quantum yield from 20% (3.5 nm) to approximately 10% (5.0 nm) as the crystal size increased.[59] Our results show that the decrease in quantum yield with an increase in crystal size is minimal, changing from φ_F = 0.0206 (2.25 nm) to φ_F = 0.0156 (2.89 nm). This is consistent with Rath *et al.*, who reported a quantum yield value of φ_F = 0.0191 for QTG QDs using the same Cd^{2+}/Se^{2-} ratio of 1.0 : 0.5 in their synthesis.[59] The relatively low decrease in quantum yield with an increase in crystal size may be related to the control exerted by the cellulose structure on TOCNs during crystal growth. Surface ligands and shell materials play a significant role in mitigating trap states. However, larger QDs have poorer ligand coverage due to their increased surface curvature. In CdSe/ZnS core–shell QDs, incomplete shell growth on larger cores leaves defects unpassivated, resulting in a lower quantum yield compared to smaller, fully passivated cores.[60]

XRD, FTIR, TEM, and TGA characterization

The crystalline nature of QTC, TOCN, and QTG QDs was investigated using X-ray diffraction (XRD). Fig. 3a presents the XRD pattern of the TOCNs and the bionanocomposite aerogel powders synthesized under the abovementioned conditions. Both materials exhibit similar peaks at 17.3°, 22.5°, and 34.6° corresponding to the crystallographic planes of (1 1 0), (2 0 0), and (0 0 4) characteristics of type I cellulose (JCPDS card no. 50-2241), space group $P21$ (no. 4).[34] The similarity in the diffraction peaks of all the analyzed compounds indicates that the formation and subsequent immobilization of the CdSe–TG QDs on the TOCNs do not affect the backbone of the oxidized cellulose nanofibers.

The diffraction peak observed at 2θ = 28° in the QTC-30 bionanocomposite sample is attributed to the (111) crystalline plane of CdS QDs (JCPDS card no. 21-0829). This transient phase is likely the result of a kinetically favored reaction wherein a small quantity of S^{2-} ions, liberated from the partial decomposition of the TG capping ligand, interacts with available Cd^{2+} ions to form CdS nuclei during the initial stages of the synthesis.[61,62] As the reaction time is extended to 60 and 90 minutes (QTC-60 and QTC-90), this peak is no longer observed. This indicates that the continuous supply of Se^{2-} ions in solution facilitates an anion exchange process, whereby the less stable S^{2-} ions are progressively displaced by Se^{2-} ions. This process ultimately converts the initial CdS into the thermodynamically more stable CdSe QDs.[63]

The diffractogram of QTG QDs (Fig. 3a) shows peaks at 25.8°, 44.3°, and 46.8° associated with lattice planes with Miller indices of (1 1 1), (2 2 0), and (3 1 1), respectively, indicating the cubic phase structure of CdSe QDs (JCPDS card no. 19-0191).[18] The noise in the XRD diffractogram can be attributed to surface defects or the formation of smaller-size QTG QDs.

© 2025 The Author(s). Published by the Royal Society of Chemistry

Open Access Article. Published on 11 September 2025. Downloaded on 12.05.2026 23:40:00.
This article is licensed under a Creative Commons Attribution-NonCommercial 3.0 Unported Licence.

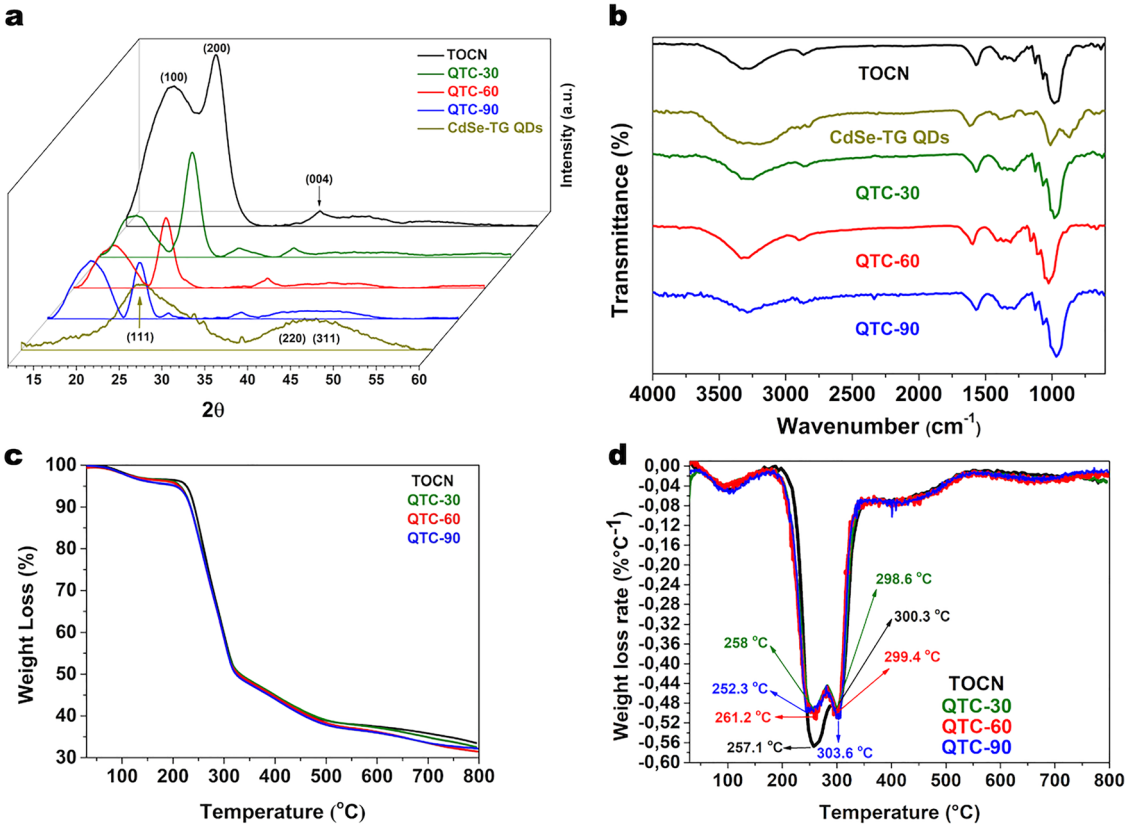

Fig. 3 (a) XRD diffractograms, (b) FTIR spectra, (c) TGA, and (d) DTG analysis for QTG QDs and QTC bionanocomposites synthesized at 30, 60, and 90 minutes.

Simultaneously, broad signals can indicate residual oxygen in the reaction medium despite performing the reaction with degassed water under an argon atmosphere. The mean crystalline diameter D for CdSe–TG QDs can be estimated according to Scherrer's formula from the full width at the half maximum (FWHM) of the crystallographic plane (1 1 1):

$$D = \frac{k\lambda}{\beta \cos\theta} \quad (2)$$

where $k = 0.9$ is an instrumental constant, λ is the wavelength of the incident X-ray of the CuK_α line (1.5405 Å), and b is the FWHM of the diffraction peak. Based on the diffraction plane (1 1 1) at $2\theta = 25.8^\circ$, the average size of CdSe–TG QDs is estimated at approximately 6.82 nm. This value is larger than that measured *via* TEM analysis (Fig. 5a) due to the uncertainty in determining the peak's width value. The mean crystalline diameter of the QDs in the bionanocomposite could not be calculated from XRD data because the CdSe–TG QD diffraction peaks were absent in the QTC diffractogram. Likewise, the crystallinity index (CrI) of TOCNs before and after the synthesis of CdSe–TG QDs NPs was calculated using the following equation:[64]

$$\mathrm{CrI}_{200} = \frac{I_{200} - I_{\mathrm{am}}}{I_{\mathrm{am}}} \times 100 \quad (3)$$

where I_{200} represents the maximum intensity of the crystalline peak from the diffraction plane (2 0 0), while I_{am} is the intensity of the amorphous diffraction. The crystallinity index for TOCNs was 46.4%, whereas the QTC bionanocomposites exhibited values of 22.3%, 15.8%, and 10.6% at 30, 60, and 90 minutes, respectively. This indicates that the crystallinity of the bionanocomposites was lower than that of the TOCNs and showed a decreasing trend as the reaction time increased. A decrease in crystallinity could be related to the *in situ* growth of CdSe QDs on the cellulose nanofiber surface, which gradually weakens the hydrogen bonds among TOCNs, resulting in an increase in amorphous content regions.[34] The effect can also be a result of the high reaction temperature, further weakening the hydrogen bond network.

The FTIR spectra of freeze-dried TOCNs and QTC bionanocomposites reveal distinct cellulose bands (Fig. 3b). A prominent band near 1600 cm^{-1} indicates the asymmetric stretching vibrations of carboxylate groups.[65] The broadband from 3000 to 3400 cm^{-1} corresponds to the stretching of the –OH group. The peaks at around 1000 and 2900 cm^{-1} are attributed to the CH_2 and C–OH stretching vibrations. The signal between 1095 and 1206 cm^{-1} is characteristic of the (1 → 4) C–O–C glucosidic bond vibration. Slight shifts in the wavenumber values were observed for most FTIR peaks in QTC compared to TOCNs (Table 2). These shifts indicate a strong interaction between the $-COO^-$ groups of TOCNs and the Cd^{2+}–TG complex, which is involved in forming CdSe–TG QDs on the cellulose nanofibers.[66] The similarity of the FTIR profiles among the

Open Access Article. Published on 11 September 2025. Downloaded on 12.05.2026 23:40:00.
This article is licensed under a Creative Commons Attribution-NonCommercial 3.0 Unported Licence.

Table 2 FTIR peaks of freeze-dried TOCNs, QTG QDs, and QTC bionanocomposites

	Wavenumber (cm^{-1})					
Sample	νC=O	νOH	νCH_2	νC–OH	νC–O–C	νCd–Se
TOCN	1567	3295	2863	977	1068	737
QTG-1	1619	3271	2832	1009		
QTC-30	1567	3279	2856	976	1095–1206	
QTC-60	1595	3311	2895	1025		
QTC-90	1568	3311	2879	973		

samples suggests that the chemical structure of TOCNs remains unchanged despite the immobilization of QD NPs.

The QTC bionanocomposites' thermogravimetric behaviour is similar to that of TOCNs, indicating that the biopolymer's structure remains intact during the synthesis. This observation aligns with the XRD and FTIR data discussed above. TGA thermograms (Fig. 3c) of TOCNs and QTC bionanocomposite aerogels reveal an initial weight loss of about 3% between 30 °C and 120 °C, attributed to the samples' humidity and residual solvent traces absorbed by the porous TOCN structure.[67] The second significant weight loss (>50%) occurs in the region of 200–400 °C, which is attributed to cellulose depolymerization to form levoglucosan and levoglucosenone in a one-step process.[68] The mass loss observed between 190 °C and 234 °C is attributed to the breakdown of the crystalline zones in TOCNs and QTC bionanocomposites, along with the decomposition of the amorphous region of the TOCN matrix into D-glucopyranose units. Subsequently, significant thermal-oxidative degradation of the polymeric structure initiates at approximately 510 °C.[69,70] As shown in Fig. 3c, the presence of CdSe–TG QDs on the TOCN polymer matrix causes a small decrease in thermal degradation temperature compared to TOCNs. Finally, the dramatic weight loss after 250 °C can be attributed to the decomposition of the carboxylic units on the TOCN surface, followed by cellulose depolymerization.[71,72] The DTG curves in Fig. 3d showed two distinct bands at approximately 260 °C and 300 °C. The former is due to thermal degradation of anhydroglucuronate units and the latter to cellulose backbone decomposition.[71] The low thermal variability in both TGA and DTG thermograms of the bionanocomposites compared to TOCNs indicates that the formation of CdSe–TG QDs on the TOCN surface does not significantly alter the cellulosic material's thermal stability.

The morphology and dispersion of the QTC bionanocomposites were examined using TEM. Fig. 4 demonstrates that CdSe–TG QDs, both with and without TOCNs, are nearly spherical and show a low tendency to agglomerate. However, the QTC-30 bionanocomposite exhibited improved dispersion of the QD NPs, as illustrated in Fig. 4b, attributed to the porous network structure of TOCNs that facilitates the anchoring and distribution of Cd^{2+} ions uniformly within the TOCN fibers. Consequently, we observe that the CdSe–TG QDs (Fig. 4a) formed larger NPs, measuring approximately 4 nm. In contrast, the QTC-30 bionanocomposite displayed a more uniform particle size of around 2.3 nm (Fig. 4b). Electron dispersive X-ray spectroscopy (EDX) was employed to confirm the elemental composition of the nanomaterials, with the detected elements aligning with those expected in the bionanocomposite structure. The intense peaks of carbon and oxygen result from the high concentration of TOCNs. The cadmium and selenium peaks arise from the formation of CdSe TG QDs, further confirmed by the presence of the sulfur peak from the 1-thioglycerol capping agent (Fig. S2).

QTC bionanocomposites as chemosensors

QTC bionanocomposites served as chemosensors for Cu^{2+} ions. Heavy metals, essential to industrial processes, can—at high concentrations—significantly pollute the environment because of their reactivity.[73] While copper is a crucial microelement aiding in energy production, connective tissue formation, and brain development, excessive levels can adversely affect the central nervous system, potentially leading to diseases like Parkinson's and Alzheimer's, along with other neuromotor system issues.[74] Thus, a straightforward approach for selectively and sensitively detecting these heavy metals in the environment is relevant. The UV-vis and fluorescence spectra of the QTC bionanocomposites were recorded in water to evaluate the absorbance and fluorescence emission intensity in response to Cu^{2+} and several other metal ions, including Ca^{2+}, Mg^{2+}, Fe^{3+}, Ni^{2+}, Zn^{2+}, and Cd^{2+}. For bionanocomposites synthesized at varying reaction times, the absorbance band at 450 nm exhibited a linear increase with Cu^{2+} addition, as depicted in Fig. 5b. As the copper concentration rose, the dip at this wavelength began to fade, resulting in a continuous line with enhanced absorbance. This trend is more clearly seen at approximately 500 nm. The absorbance spectra revealed a linear response to Cu^{2+} ions for each bionanocomposite within a range of 0–12.8 ppm (refer to Table S2).

Fig. 5b and d show that QTC-30 achieved the lowest detection limit (LOD) along with the highest R^2 coefficient and sensitivity in both absorbance and fluorescence measurement modes. The LOD, sensitivity, and R^2 coefficient values of QTC-60 and QTC-90 bionanocomposites suggest that they both perform similarly, but not as well as QTC-30. These results indicate that reaction time affects the LOD and sensitivity in QTC bionanocomposites. The LOD was calculated using $3\sigma/K$ as per IUPAC standards, where σ is the standard deviation of ten measurements of the material's absorbance in the absence of Cu^{2+}.[75]

The selectivity of the QTC bionanocomposites was also evaluated using UV-vis spectroscopy to analyze the impact of different metal ions on the optical response of the chemosensor. Thus, the absorbance of the bionanocomposites was titrated with various metal ions within a concentration range of 0 ppm to 5.5 ppm. As illustrated in Fig. 5a, only the Cu^{2+} ions resulted in a significant change in absorbance. In contrast, the other metal ions had minimal effect on the absorbance of the chemosensors. Therefore, QTC bionanocomposites could serve as a practical absorbance probe for the selective detection of Cu^{2+} compared to commonly found water ions such as Fe^{3+}, Ni^{2+}, Zn^{2+}, and Cd^{2+}. Fig. S4 and Fig. 5c display the fluorescence

© 2025 The Author(s). Published by the Royal Society of Chemistry

Open Access Article. Published on 11 September 2025. Downloaded on 12.05.2026 23:40:00.
This article is licensed under a Creative Commons Attribution-NonCommercial 3.0 Unported Licence.

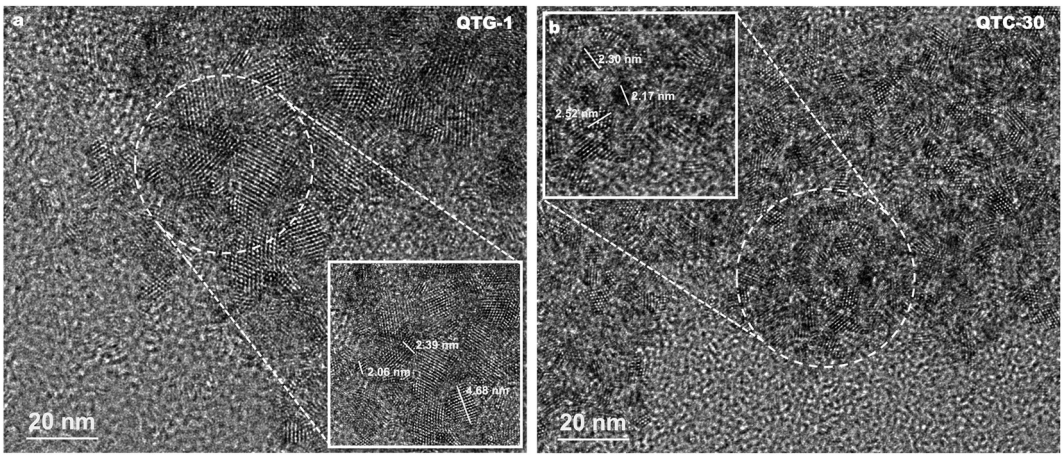

Fig. 4 TEM images of the (a) QTG-1 sample and the (b) QTC-30 bionanocomposite.

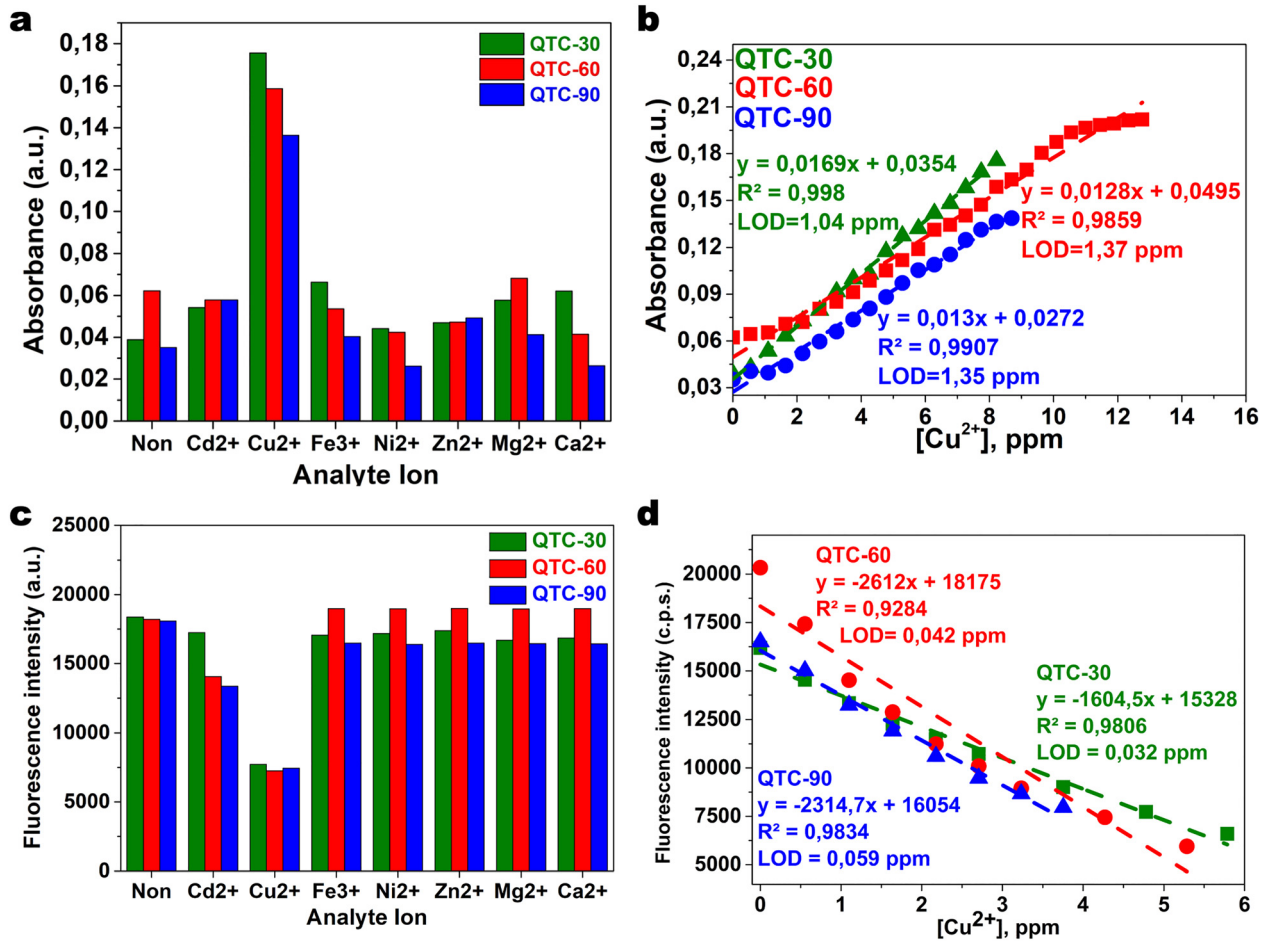

Fig. 5 Changes in (a) UV-vis absorbance and (c) fluorescence of the QTC interacting with various metal ions. Linear dynamic ranges and limits of detection (LOD) for Cu^{2+} ions using QTC bionanocomposites in (b) UV-vis absorbance and (d) fluorescence measurement modes.

emission spectra and fluorescence quenching for the QTC bionanocomposites with the metal ions listed above, at an excitation wavelength of 370 nm. Similar to the findings in UV-vis spectroscopy, the QTC-30 bionanocomposite exhibited the lowest limit of detection for Cu^{2+} ions, as illustrated in Fig. 5d. In contrast, the other biocomposites showed higher LOD values, possibly due to the larger size of the CdSe–TG QDs on the TOCN scaffold. This observation is supported by the

Open Access Article. Published on 11 September 2025. Downloaded on 12.05.2026 23:40:00.
This article is licensed under a Creative Commons Attribution-NonCommercial 3.0 Unported Licence.

research of Zhong *et al.*, who noted that larger NPs result in reduced sensitivity when quenching the photoluminescence of CdTe QDs with various metal ions. According to these authors, the increase in Cu^{2+} concentration leads to its reduction to Cu^{+}, which ultimately displaces Cd on the QD surface through cation exchange, causing fluorescence quenching due to surface defects.[76] Fig. 5c shows that only Cu^{2+} and Cd^{2+} could quench the chemosensors' fluorescence to some extent.

Interestingly, after a specific concentration (*e.g.*, QTC-30 at 14.1 ppm Cu^{2+} and 5.8 ppm Cd^{2+}), the intensity of the fluorescence emission remains unchanged. This could be attributed to the formation of CdSe–TG QDs within the TOCN network, which may not interact with the metal ions, as well as the Cu^{+} ions possibly being unable to replace the Cd on the surface of the QDs.

Conclusions

This study successfully demonstrates the preparation of CdSe–TG quantum dots (QDs) using TEMPO-oxidized cellulose nanofibers (TOCNs) as both a capping and reducing agent in an aqueous environment under mild conditions. The rapid synthesis of QTC bionanocomposites within thirty minutes marks a significant advancement, reducing the reaction time from previously reported reaction times (up to twelve hours) when employing $NaBH_4$. This remarkable efficiency reveals the potential of residual aldehydes in TOCNs to effectively reduce selenium cations, facilitating the formation of CdSe QDs.

Transmission electron microscopy (TEM) micrographs reveal enhanced control over nanocrystal growth facilitated by TOCNs, yielding nanoparticles with an average diameter of approximately 2.3 nm. The fluorescence emission of the bionanocomposites was observed at around 545 nm, with an excitation wavelength of 390 nm. Notably, the well-dispersed formation of QDs on the TOCN surface contributes to a significantly intense fluorescence observable to the naked eye.

The CdSe–TG QDs/TOCN (QTC) biocomposites serve as effective chemosensors for detecting copper cations in aqueous solutions, exhibiting exceptional selectivity towards Cu^{2+} ions, even amidst other metal cations. This selectivity is substantiated through rigorous testing *via* UV-vis and fluorescence spectroscopy. While a slight fluorescence quenching was noted in the presence of Cd^{2+} ions, particularly for chemosensors synthesized at 60 and 90 minutes, the QTC-30 variant showcased an impressive detection limit of 320 ppb for Cu^{2+} detection. This finding positions the QTC bionanocomposites as promising candidates for developing more robust and sensitive probes for copper ion detection in aqueous environments, paving the way for future advancements in sensor technology.

Declaration AI and AI-assisted technologies in the writing process

During the preparation of this work, the authors utilized Grammarly Editor v1.120.0.0 and OpenAI's ChatGPT to enhance language and clarity during the manuscript drafting process. After using these tools, the authors reviewed and edited the text as needed. All intellectual content and conclusions are the authors' own.

Author contributions

Conceptualization: M. Y. C. and C. B. T.; methodology, data curation and data analysis: D. A. A., M. Y. C., C. B. T., and M. C. C.; formal analysis and investigation: M. C. C. and D. A. A.; validation: M. Y. C. and C. B. T.; writing – original draft preparation: M. C. C.; writing – review and editing: M. C. C. and M. Y. C.; and supervision: C. B. T. and M. Y. C. All the authors discussed and contributed to this work.

Conflicts of interest

The authors declare that they have no conflicts of interest.

Data availability

Data will be made available on request.

Supplementary information available: Characterization of QDs synthesis-dependent properties and their chemosensing performance for detecting Cu and Cd ions. See DOI: **https://doi.org/10.1039/d5ma00700c**.

Acknowledgements

We thank the Central Research Laboratory at Universidad Industrial de Santander – Guatiguará Technological Park for infrastructural support. We also acknowledge financial support from the SGR-Gobernación de Santander Grant BPIN 2020000100351 and the SGR-Gobernación de Santander Grant BPIN 2020000100258.

References

1 G. H. Carey, A. L. Abdelhady, Z. Ning, S. M. Thon, O. M. Bakr and E. H. Sargent, Colloidal Quantum Dot Solar Cells, *Chem. Rev.*, 2015, 12732–12763, DOI: **10.1021/acs.chemrev.5b00063**.

2 K. Kaviyarasu, A. Ayeshamariam, E. Manikandan, J. Kennedy, R. Ladchumananandasivam, U. Umbelino Gomes, M. Jayachandran and M. Maaza, Solution Processing of CuSe Quantum Dots: Photocatalytic Activity under RhB for UV and Visible-Light Solar Irradiation, *Mater. Sci. Eng., B*, 2016, **210**, 1–9, DOI: **10.1016/j.mseb.2016.05.002**.

3 N. Ben Brahim, N. B. H. Mohamed, M. Echabaane, M. Haouari, R. Ben Chaâbane, M. Negrerie and H. Ben Ouada, Thioglycerol-Functionalized CdSe Quantum Dots Detecting Cadmium Ions, *Sens. Actuators, B*, 2015, **220**, 1346–1353, DOI: **10.1016/j.snb.2015.07.049**.

4 M. Ali, D. Zayed, W. Ramadan, O. A. Kamel, M. Shehab and S. Ebrahim, Synthesis, Characterization and Cytotoxicity of

© 2025 The Author(s). Published by the Royal Society of Chemistry

Open Access Article. Published on 11 September 2025. Downloaded on 12.05.2026 23:40:00.
This article is licensed under a Creative Commons Attribution-NonCommercial 3.0 Unported Licence.

Polyethylene Glycol-Encapsulated CdTe Quantum Dots, *Int. Nano Lett.*, 2019, **9**(1), 61–71, DOI: 10.1007/s40089-018-0262-2.

5 S. K. Mahto, T. H. Yoon and S. W. Rhee, Cytotoxic Effects of Surface-Modified Quantum Dots on Neuron-like PC12 Cells Cultured inside Microfluidic Devices, *Biochip. J.*, 2010, **4**(1), 82–88, DOI: 10.1007/s13206-010-4113-0.

6 N. J. Niemuth, D. N. Williams, A. C. Mensch, Y. Cui, G. Orr, Z. Rosenzweig and R. D. Klaper, Redesign of Hydrophobic Quantum Dots Mitigates Ligand-Dependent Toxicity in the Nematode C. Elegans, *NanoImpact*, 2021, 22, DOI: 10.1016/j.impact.2021.100318.

7 L. Jing, S. v Kershaw, Y. Li, X. Huang, Y. Li, A. L. Rogach and M. Gao, Aqueous Based Semiconductor Nanocrystals, *Chem. Rev.*, 2016, 10623–10730, DOI: 10.1021/acs.chemrev.6b00041.

8 H. Arshad, M. Chaudhry, S. Mehmood, A. Farooq, M. Wang and A. S. Bhatti, The Electrochemical Reaction Controlled Optical Response of Cholestrol Oxidase (COx) Conjugated CdSe/ZnS Quantum Dots, *Sci. Rep.*, 2020, **10**(1), 1–10, DOI: 10.1038/s41598-020-77499-9.

9 N. ben Brahim, N. Bel Haj Mohamed, M. Poggi, R. ben Chaâbane, M. Haouari, H. ben Ouada and M. Negrerie, Interaction of L-Cysteine Functionalized CdSe Quantum Dots with Metallic Cations and Selective Binding of Cobalt in Water Probed by Fluorescence, *Sens. Actuators, B*, 2017, **243**, 489–499, DOI: 10.1016/j.snb.2016.12.003.

10 A. S. Schulze, I. Tavernaro, F. Machka, O. Dakischew, K. S. Lips and M. S. Wickleder, Tuning Optical Properties of Water-Soluble CdTe Quantum Dots for Biological Applications, *J. Nanopart. Res.*, 2017, **19**(2), 70, DOI: 10.1007/s11051-017-3757-2.

11 L. S. V. Barbosa, L. S. G. Teixeira, M. G. A. Korn and R. M. M. Santana, Evaluation of the Direct Interaction between Amino Acids and Glutathione-Coated CdTe Quantum Dots and Application in Urinalysis for Histidine Determination, *J. Braz. Chem. Soc.*, 2021, **32**(3), 588–598, DOI: 10.21577/0103-5053.20200212.

12 S. N. Wang, J. Zhu, X. Li, J. J. Li and J. W. Zhao, Fluorescence Turn-on Sensing of Trace Cadmium Ions Based on EDTA-Etched CdTe@CdS Quantum Dot, *Spectrochim. Acta, Part A*, 2018, **201**, 119–127, DOI: 10.1016/j.saa.2018.04.065.

13 Q. Wu, M. Zhou, J. Shi, Q. Li, M. Yang and Z. Zhang, Synthesis of Water-Soluble Ag_2S Quantum Dots with Fluorescence in the Second Near-Infrared Window for Turn-on Detection of Zn(II) and Cd(II), *Anal. Chem.*, 2017, **89**(12), 6616–6623, DOI: 10.1021/acs.analchem.7b00777.

14 J. Kaur, Komal, Renu, V. Kumar, K. B. Tikoo, S. Bansal, A. Kaushik and S. Singhal, Glutathione Modified Fluorescent CdS QDs Synthesized Using Environmentally Benign Pathway for Detection of Mercury Ions in Aqueous Phase, *J. Fluoresc.*, 2020, **30**(4), 773–785, DOI: 10.1007/s10895-020-02545-8.

15 K. Valadi, S. Gharibi, R. Taheri-Ledari, S. Akin, A. Maleki and A. E. Shalan, Metal Oxide Electron Transport Materials for Perovskite Solar Cells: A Review, *Environ. Chem. Lett.*, 2021, 2185–2207, DOI: 10.1007/s10311-020-01171-x.

16 T. Baines, G. Zoppi, L. Bowen, T. P. Shalvey, S. Mariotti, K. Durose and J. D. Major, Incorporation of CdSe Layers into CdTe Thin Film Solar Cells, *Sol. Energy Mater. Sol. Cells*, 2018, **180**, 196–204, DOI: 10.1016/j.solmat.2018.03.010.

17 A. Kumari, A. Sharma, U. Malairaman and R. R. Singh, Proficient Surface Modification of CdSe Quantum Dots for Highly Luminescent and Biocompatible Probes for Bioimaging: A Comparative Experimental Investigation, *J. Lumin.*, 2018, **199**, 174–182, DOI: 10.1016/j.jlumin.2018.03.032.

18 N. ben Brahim, N. Bel Haj Mohamed, M. Poggi, R. ben Chaâbane, M. Haouari, H. ben Ouada and M. Negrerie, Interaction of L-Cysteine Functionalized CdSe Quantum Dots with Metallic Cations and Selective Binding of Cobalt in Water Probed by Fluorescence, *Sens. Actuators, B*, 2017, **243**, 489–499, DOI: 10.1016/j.snb.2016.12.003.

19 S. Jiang, Z. Lu, T. Su, Y. Feng, C. Zhou, P. Hong, S. Sun and C. Li, High Sensitivity Detection of Copper Ions in Oysters Based on the Fluorescence Property of Cadmium Selenide Quantum Dots, *Chemosensors*, 2019, **7**(4), 47, DOI: 10.3390/chemosensors7040047.

20 B. Karimi, M. Shafiee Afarani and A. M. Arabi, Hydrothermal Synthesis of Cadmium Selenide Quantum Dots: Effect of Reducing Agent, *Appl. Phys. A: Mater. Sci. Process.*, 2020, **126**(9), 706, DOI: 10.1007/s00339-020-03903-w.

21 M. L. Chacón-Patiño, C. Blanco-Tirado, J. P. Hinestroza and M. Y. Combariza, Biocomposite of Nanostructured MnO2 and Fique Fibers for Efficient Dye Degradation, *Green Chem.*, 2013, **15**(10), 2920–2928, DOI: 10.1039/c3gc40911b.

22 L. A. Calderón-Vergara, S. A. Ovalle-Serrano, C. Blanco-Tirado and M. Y. Combariza, Influence of Post-Oxidation Reactions on the Physicochemical Properties of TEMPO-Oxidized Cellulose Nanofibers before and after Amidation, *Cellulose*, 2020, **27**(3), 1273–1288, DOI: 10.1007/s10570-019-02849-4.

23 F. N. Gómez, M. Y. Combariza and C. Blanco-Tirado, Facile Cellulose Nanofibrils Amidation Using a 'One-Pot' Approach, *Cellulose*, 2017, **24**(2), 717–730, DOI: 10.1007/s10570-016-1174-9.

24 X. Jiao, K. Jia, Y. Yu, D. Liu, J. Zhang, K. Zhang, H. Zheng, X. Sun, Y. Tong, Q. Wei and P. Lv, Nanocellulose-Based Functional Materials towards Water Treatment, *Carbohydr. Polym.*, 2025, **350**, 122977, DOI: 10.1016/j.carbpol.2024.122977.

25 M. Ghasemlou, F. Daver, E. P. Ivanova, Y. Habibi and B. Adhikari, Surface Modifications of Nanocellulose: From Synthesis to High-Performance Nanocomposites, *Prog. Polym. Sci.*, 2021, **119**, 101418, DOI: 10.1016/j.progpolymsci.2021.101418.

26 Y. Qi, Y. Guo, A. A. Liza, G. Yang, M. H. Sipponen, J. Guo and H. Li, Nanocellulose: A Review on Preparation Routes and Applications in Functional Materials, *Cellulose*, 2023, **30**(7), 4115–4147, DOI: 10.1007/s10570-023-05169-w.

27 A. Isogai, T. Saito and H. Fukuzumi, TEMPO-Oxidized Cellulose Nanofibers, *Nanoscale*, 2011, 71–85, DOI: 10.1039/c0nr00583e.

28 C. Yan, Z. Fang, A. Tang, W. Liu, Y. Liu and H. Shi, A Tunable Optoelectronic Nanofibrillated Cellulose/CdS Quantum Dot Film with Improved Transmittance and Strength, *Cellulose*, 2018, **25**(4), 2405–2417, DOI: 10.1007/s10570-018-1727-1.

Open Access Article. Published on 11 September 2025. Downloaded on 12.05.2026 23:40:00.
This article is licensed under a Creative Commons Attribution-NonCommercial 3.0 Unported Licence.

29 Q. Guan, R. Song, W. Wu, L. Zhang, Y. Jing, H. Dai and G. Fang, Fluorescent CdTe-QD-Encoded Nanocellulose Microspheres by Green Spraying Method, *Cellulose*, 2018, **25**(12), 7017–7029, DOI: **10.1007/s10570-018-2065-z**.

30 Y. Ge, S. Chen, J. Yang, B. Wang and H. Wang, Color-Tunable Luminescent CdTe Quantum Dot Membranes Based on Bacterial Cellulose (BC) and Application in Ion Detection, *RSC Adv.*, 2015, **5**(69), 55756–55761, DOI: **10.1039/C5RA08361C**.

31 X. Li and Y. Hu, Luminescent Films Functionalized with Cellulose Nanofibrils/CdTe Quantum Dots for Anti-Counterfeiting Applications, *Carbohydr. Polym.*, 2019, **203**, 167–175, DOI: **10.1016/j.carbpol.2018.09.028**.

32 L. Valencia, S. Kumar, E. M. Nomena, G. Salazar-Alvarez and A. P. Mathew, In-Situ Growth of Metal Oxide Nanoparticles on Cellulose Nanofibrils for Dye Removal and Antimicrobial Applications, *ACS Appl. Nano Mater.*, 2020, **3**(7), 7172–7181, DOI: **10.1021/acsanm.0c01511**.

33 K. Benaissi, L. Johnson, D. A. Walsh and W. Thielemans, Synthesis of Platinum Nanoparticles Using Cellulosic Reducing Agents, *Green Chem.*, 2010, **12**(2), 220–222, DOI: **10.1039/b913218j**.

34 S. A. Ovalle-Serrano, L. A. Díaz-Serrano, C. Hong, J. P. Hinestroza, C. Blanco-Tirado and M. Y. Combariza, Synthesis of Cellulose Nanofiber Hydrogels from Fique Tow and Ag Nanoparticles, *Cellulose*, 2020, **27**(17), 9947–9961, DOI: **10.1007/s10570-020-03527-6**.

35 F. Séby, M. Potin-Gautier, E. Giffaut, G. Borge and O. F. X. Donard, A Critical Review of Thermodynamic Data for Selenium Species at 25 °C, *Chem. Geol.*, 2001, **171**(3–4), 173–194, DOI: **10.1016/S0009-2541(00)00246-1**.

36 S. Jiang, Z. Lu, T. Su, Y. Feng, C. Zhou, P. Hong, S. Sun and C. Li, High Sensitivity Detection of Copper Ions in Oysters Based on the Fluorescence Property of Cadmium Selenide Quantum Dots, *Chemosensors*, 2019, **7**(4), 47, DOI: **10.3390/chemosensors7040047**.

37 A. M. Brouwer, Standards for Photoluminescence Quantum Yield Measurements in Solution (IUPAC Technical Report), *Pure Appl. Chem.*, 2011, **83**(12), 2213–2228, DOI: **10.1351/PAC-REP-10-09-31**.

38 M. G. González, Determination of the Photoluminescence Quantum Yield of Diluted Dye Solutions in Highly Scattering Media by Pulsed Photoacoustic Spectroscopy, *Appl. Opt.*, 2010, **49**(36), 6850–6854, DOI: **10.1364/AO.49.006850**.

39 P. Cook, Y. Kim, K. Yuan, M. C. Marcano and U. Becker, Electrochemical, Spectroscopic, and Computational Investigations on Redox Reactions of Selenium Species on Galena Surfaces, *Minerals*, 2019, **9**(7), 437, DOI: **10.3390/min9070437**.

40 V. S. Saji and C.-W. Lee, Selenium Electrochemistry, *RSC Adv.*, 2013, **3**(26), 10058, DOI: **10.1039/c3ra40678d**.

41 D. Pawcenis, D. K. Chlebda, R. J. Jędrzejczyk, M. Leśniak, M. Sitarz and J. Łojewska, Preparation of Silver Nanoparticles Using Different Fractions of TEMPO-Oxidized Nanocellulose, *Eur. Polym. J.*, 2019, **116**, 242–255, DOI: **10.1016/j.eurpolymj.2019.04.022**.

42 H. Yu, L. Zheng, T. Zhang, J. Ren, W. Cheng, L. Zhang and P. Meng, Adsorption Behavior of Cd (II) on TEMPO-Oxidized Cellulose in Inorganic/Organic Complex Systems, *Environ. Res.*, 2021, **195**, 110848, DOI: **10.1016/j.envres.2021.110848**.

43 S. G. Bratsch, Standard Electrode Potentials and Temperature Coefficients in Water at 298.15 K, *J. Phys. Chem. Ref. Data*, 1989, **18**(1), 1–21, DOI: **10.1063/1.555839**.

44 S. Katiyar, S. Chang, I. Ullah, W. Hou, A. Conde-Delmoral, S. Qiu, G. Morell and X. Wu, Unlocking the Potential of Cadmium Plating Chemistry for Low-Polarization, Long-Cycling, and Ultrahigh-Efficiency Aqueous Metal Batteries, *Energy Environ. Sci.*, 2024, **17**(13), 4770–4779, DOI: **10.1039/D4EE01615G**.

45 J. F. Gomes, A. C. Garcia, E. B. Ferreira, C. Pires, V. L. Oliveira, G. Tremiliosi-Filho and L. H. S. Gasparotto, New Insights into the Formation Mechanism of Ag, Au and AgAu Nanoparticles in Aqueous Alkaline Media: Alkoxides from Alcohols, Aldehydes and Ketones as Universal Reducing Agents, *Phys. Chem. Chem. Phys.*, 2015, **17**(33), 21683–21693, DOI: **10.1039/c5cp02155c**.

46 S. Nath, S. K. Ghosh, S. Panigrahi and T. Pal, Aldehyde Assisted Wet Chemical Route to Synthesize Gold Nanoparticles, *Indian J. Chem.*, 2004, **43**, 1147–1151.

47 Q. Xu, L. Jin, Y. Wang, H. Chen and M. Qin, Synthesis of Silver Nanoparticles Using Dialdehyde Cellulose Nanocrystal as a Multi-Functional Agent and Application to Antibacterial Paper, *Cellulose*, 2019, **26**(2), 1309–1321, DOI: **10.1007/s10570-018-2118-3**.

48 L. Riva, A. Dotti, G. Iucci, I. Venditti, C. Meneghini, I. Corsi, I. Khalakhan, G. Nicastro, C. Punta and C. Battocchio, Silver Nanoparticles Supported onto TEMPO-Oxidized Cellulose Nanofibers for Promoting Cd^{2+} Cation Adsorption, *ACS Appl. Nano Mater.*, 2024, **7**(2), 2401–2413, DOI: **10.1021/acsanm.3c06052**.

49 N. Ben Brahim, M. Poggi, N. B. Haj Mohamed, R. Ben Chaâbane, M. Haouari, M. Negrerie and H. Ben Ouada, Synthesis, Characterization and Spectral Temperature-Dependence of Thioglycerol-CdSe Nanocrystals, *J. Lumin.*, 2016, **177**, 402–408, DOI: **10.1016/j.jlumin.2016.05.026**.

50 J. S. Kamal, A. Omari, K. Van Hoecke, Q. Zhao, A. Vantomme, F. Vanhaecke, R. K. Capek and Z. Hens, Size-Dependent Optical Properties of Zinc Blende Cadmium Telluride Quantum Dots, *J. Phys. Chem. C*, 2012, **116**(8), 5049–5054.

51 J. Jasieniak, L. Smith, J. van Embden, P. Mulvaney and M. Califano, Re-Examination of the Size-Dependent Absorption Properties of CdSe Quantum Dots, *J. Phys. Chem. C*, 2009, **113**(45), 19468–19474, DOI: **10.1021/jp906827m**.

52 Z. Zhou, G. J. Bedwell, R. Li, P. E. Prevelige and A. Gupta, Formation Mechanism of Chalcogenide Nanocrystals Confined inside Genetically Engineered Virus-like Particles, *Sci. Rep.*, 2014, 4, DOI: **10.1038/srep03832**.

53 L. Chen, C. Lai, R. Marchewka, R. M. Berry and K. C. Tam, Use of CdS Quantum Dot-Functionalized Cellulose Nanocrystal Films for Anti-Counterfeiting Applications, *Nanoscale*, 2016, **8**(27), 13288–13296, DOI: **10.1039/C6NR03039D**.

© 2025 The Author(s). Published by the Royal Society of Chemistry

Open Access Article. Published on 11 September 2025. Downloaded on 12.05.2026 23:40:00.
This article is licensed under a Creative Commons Attribution-NonCommercial 3.0 Unported Licence.

54 U. e Kalsoom, R. Yi, J. Qu and L. Liu, Nonlinear Optical Properties of CdSe and CdTe Core-Shell Quantum Dots and Their Applications, *Front. Phys.*, 2021, 9, DOI: 10.3389/fphy.2021.612070.

55 M. A. Hegazy and A. M. Abd El-Hameed, Characterization of CdSe-Nanocrystals Used in Semiconductors for Aerospace Applications: Production and Optical Properties, *NRIAG J. Astron. Geophys.*, 2014, 3(1), 82–87, DOI: 10.1016/j.nrjag.2014.05.002.

56 D. Pawcenis, E. Twardowska, M. Leśniak, R. J. Jędrzejczyk, M. Sitarz and J. Profic-Paczkowska, TEMPO-Oxidized Cellulose for in Situ Synthesis of Pt Nanoparticles. Study of Catalytic and Antimicrobial Properties, *Int. J. Biol. Macromol.*, 2022, **213**, 738–750, DOI: 10.1016/j.ijbiomac.2022.06.020.

57 M. Kuno, I. Gushchina, S. Toso and V. Trepalin, No One Size Fits All: Semiconductor Nanocrystal Sizing Curves, *J. Phys. Chem. C*, 2022, **126**(29), 11867–11874, DOI: 10.1021/acs.jpcc.2c04734.

58 E. V. Kolobkova, N. V. Nikonorov, M. S. Kuznetsova and M. N. Bataev, Controlling the Luminescence of CdSe Quantum Dots in the Fluorinephosphate Glass, *J. Non-Cryst. Solids*, 2024, **646**, 123248, DOI: 10.1016/j.jnoncrysol.2024.123248.

59 A. Singh, V. S. Tripathi, S. Neogy and M. C. Rath, Facile and Green Synthesis of 1-Thioglycerol Capped CdSe Quantum Dots in Aqueous Solution, *Mater. Chem. Phys.*, 2018, **214**, 320–329, DOI: 10.1016/j.matchemphys.2018.04.116.

60 U. e Kalsoom, R. Yi, J. Qu and L. Liu, Nonlinear Optical Properties of CdSe and CdTe Core-Shell Quantum Dots and Their Applications, *Front. Phys.*, 2021, 9, DOI: 10.3389/fphy.2021.612070.

61 C. Unni, D. Philip and K. G. Gopchandran, Studies on Optical Absorption and Photoluminescence of Thioglycerol-Stabilized ZnS Nanoparticles, *Opt. Mater.*, 2009, **32**(1), 169–175, DOI: 10.1016/j.optmat.2009.06.019.

62 Y. Ge, S. Chen, J. Yang, B. Wang and H. Wang, Color-Tunable Luminescent CdTe Quantum Dot Membranes Based on Bacterial Cellulose (BC) and Application in Ion Detection, *RSC Adv.*, 2015, **5**(69), 55756–55761, DOI: 10.1039/C5RA08361C.

63 X. Kong, Y. Deng, Y. Zou, J. Ge and Y. Wang, Anion Exchange in Semiconductor Magic-Size Clusters, *J. Am. Chem. Soc.*, 2024, **146**(8), 5445–5454, DOI: 10.1021/jacs.3c12853.

64 L. Segal, J. J. Creely, A. E. Martin and C. M. Conrad, An Empirical Method for Estimating the Degree of Crystallinity of Native Cellulose Using the X-Ray Diffractometer, *Text. Res. J.*, 1959, **29**(10), 786–794, DOI: 10.1177/004051755902901003.

65 Z. Tang, W. Li, X. Lin, H. Xiao, Q. Miao, L. Huang, L. Chen and H. Wu, TEMPO-Oxidized Cellulose with High Degree of Oxidation, *Polymers*, 2017, **9**(9), 421, DOI: 10.3390/polym9090421.

66 F. K. Algethami, I. Saidi, H. Ben Jannet, M. Khairy, B. Y. Abdulkhair, Y. O. Al-Ghamdi and H. N. Abdelhamid, Chitosan-CdS Quantum Dots Biohybrid for Highly Selective Interaction with Copper(II) Ions, *ACS Omega*, 2022, **7**(24), 21014–21024, DOI: 10.1021/acsomega.2c01793.

67 F. Jiang and Y. L. Hsieh, Chemically and Mechanically Isolated Nanocellulose and Their Self-Assembled Structures, *Carbohydr. Polym.*, 2013, **95**(1), 32–40, DOI: 10.1016/j.carbpol.2013.02.022.

68 V. Piazza, R. B. da Silva Junior, A. Frassoldati, L. Lietti, S. Chiaberge, C. Gambaro, A. Siviero, T. Faravelli and A. Beretta, Detailed Speciation of Biomass Pyrolysis Products with a Novel TGA-Based Methodology: The Case-Study of Cellulose, *J. Anal. Appl. Pyrolysis*, 2024, **178**, 106413, DOI: 10.1016/j.jaap.2024.106413.

69 J. George, K. V. Ramana, S. N. Sabapathy, J. H. Jagannath and A. S. Bawa, Characterization of Chemically Treated Bacterial (Acetobacter Xylinum) Biopolymer: Some Thermo-Mechanical Properties, *Int. J. Biol. Macromol.*, 2005, **37**(4), 189–194, DOI: 10.1016/j.ijbiomac.2005.10.007.

70 K. Jradi, B. Bideau, B. Chabot and C. Daneault, Characterization of Conductive Composite Films Based on TEMPO-Oxidized Cellulose Nanofibers and Polypyrrole, *J. Mater. Sci.*, 2012, **47**(8), 3752–3762, DOI: 10.1007/s10853-011-6226-9.

71 H. Fukuzumi, T. Saito, Y. Okita and A. Isogai, Thermal Stabilization of TEMPO-Oxidized Cellulose, *Polym. Degrad. Stab.*, 2010, **95**(9), 1502–1508, DOI: 10.1016/j.polymdegradstab.2010.06.015.

72 C. Du, H. Li, B. Li, M. Liu and H. Zhan, Characteristics and Properties of Cellulose Nanofibers Prepared by TEMPO Oxidation of Corn Husk, *BioResources*, 2016, **11**(2), 5276–5284, DOI: 10.15376/biores.11.2.5276-5284.

73 T. E. Oladimeji, M. Oyedemi, M. E. Emetere, O. Agboola, J. B. Adeoye and O. A. Odunlami, Review on the Impact of Heavy Metals from Industrial Wastewater Effluent and Removal Technologies, *Heliyon*, 2024, **10**(23), e40370, DOI: 10.1016/j.heliyon.2024.e40370.

74 G. Gromadzka, B. Tarnacka, A. Flaga and A. Adamczyk, Copper Dyshomeostasis in Neurodegenerative Diseases—Therapeutic Implications, *Int. J. Mol. Sci.*, 2020, **21**(23), 9259, DOI: 10.3390/ijms21239259.

75 G. L. Long and J. D. Winefordner, Limit of Detection A Closer Look at the IUPAC Definition, *Anal. Chem.*, 1983, **55**(07), 712A–724A, DOI: 10.1021/ac00258a724.

76 A. Wang, L. Fu, T. Rao, W. Cai, M. F. Yuen and J. Zhong, Effect of Metal Ions on the Quenching of Photoluminescent CdTe QDs and Their Recovery, *Opt. Mater.*, 2015, **42**, 548–552, DOI: 10.1016/j.optmat.2015.01.010.